Carbohydrate Polymers 97 (2013) 363–367

Contents lists available at SciVerse ScienceDirect

Carbohydrate Polymers

journal homepage: www.elsevier.com/locate/carbpol

Simple preparation of chitosan nanofibers from dry chitosan powder by the Star Burst system

Ajoy Kumar Dutta[a], Naoki Kawamoto[a], Gaku Sugino[b], Hironori Izawa[a], Minoru Morimoto[c], Hiroyuki Saimoto[a], Shinsuke Ifuku[a,*]

[a] Department of Chemistry and Biotechnology, Tottori University, Tottori 680-8502, Japan
[b] Sugino Machine Limited, 2410 Hongo, Uozu, Toyama 937-8511, Japan
[c] Research Center for Bioscience and Technology, Tottori University, Tottori 680-8500, Japan

ARTICLE INFO

Article history:
Received 21 March 2013
Received in revised form 30 April 2013
Accepted 7 May 2013
Available online 13 May 2013

Keywords:
Chitosan
Nanofibers
Star Burst

ABSTRACT

Chitosan nanofibers were easily prepared from dry chitosan powder using the Star Burst system, which employs a high-pressure water jet system. Although the chitosan nanofibers became thinner as the number of Star Burst passes increased, the fiber thickness did not change significantly above 10 passes. Crystallinity and the chitosan nanofiber length decreased after extensive treatment due to the strong collision forces breaking the fibers. The mechanical properties and thermal expansion of the chitosan nanofiber sheets were improved by increasing the number of passes up to 10, but further treatment resulted in a deterioration of these properties.

1. Introduction

Chitosan is produced by deacetylation of chitin, which is the main component of exoskeletons of crustaceans such as crab and shrimp. Chitosan has a cationic linear polysaccharide structure composed of a β-(1-4)-linked 2-amino-2-deoxy-D-glucopyranose polymer. Due to its biocompatibility and biodegradability as well as its cellular-binding, wound-healing, anti-bacterial, and anti-fungal properties, chitosan has great potential for many uses, including food, cosmetic, biomedical, and pharmaceutical applications (Muzzarelli et al., 2012; Muzzarelli, 2011, 2012; Peter, 1995; Rao & Sharma, 1997).

Nanofibers are basically defined as fibers with diameters less than 100 nanometers and an aspect ratio of more than 100 (Li & Xia, 2004; Xia et al., 2003). Due to their characteristic morphology, nanofibers are different from micro-sized fibers with regard to their dimensional, optical, and mechanical properties. Preparation of nanofibers is therefore an important subject. The electro-spinning process enables the artificial production of nanofibers from a wide range of natural polymer solutions using interactions between fluid dynamics, electrically charged surfaces, and electrically charged liquids (Huang, Zhang, Kotaki, & Ramakrishna, 2003; Lee, Jeong, Kang, Lee, & Park, 2009; Sill & Recum, 2008). However, electrospinning of chitosan itself is difficult due to its polycationic nature. The cationic charge increases the excessive surface tension of the solution (Min et al., 2004), meaning that a higher electrical force is required for nanofiber production. Another synthetic polymer is therefore usually mixed with chitosan to improve its electrospinnability (Duan, Dong, Yuan, & Yao, 2004; Lin, Fang, Wang, Cheng, & Wang, 2006).

In recent years we have prepared chitin nanofibers from a commercial chitin powder produced from crab shell (Ifuku et al., 2011). Crab shell has a hierarchical organization with various structural levels made up of chitin nanofibers (Chen, Lin, McKittrick, & Meyers, 2008; Fabritius et al., 2011; Nikolov et al., 2011; Raabe, Sachs, & Romano, 2005; Raabe et al., 2006). Since the chitin powder is made up of regularly structured chitin nanofiber aggregates, it can be downsized to nanofibers using a very simple disintegration system called Star Burst (Dutta et al., 2013; Ifuku, Yamada, Morimoto, & Saimoto, 2012; Kose & Kondo, 2011). This system employs a high-pressure water jet technology and has been used to break down various materials. The chitin nanofibers obtained from the commercial chitin powder have a highly uniform network morphology 10–20 nm in width. If the characteristic nanofiber structure of chitin could be maintained after deacetylation, nano-fibrillation of chitin using the Star Burst system could be utilized for chitosan. In this study, we report the nano-fibrillation of chitosan with 1–50 passes of the Star Burst system in water and characterize the

* Corresponding author at: Department of Chemistry and Biotechnology, Tottori University, 4-101 Koyama-cho Minami, Tottori 680-8502, Japan.
Tel.: +81 857 31 5592; fax: +81 857 31 5813.
E-mail address: sifuku@chem.tottori-u.ac.jp (S. Ifuku).

0144-8617/$ – see front matter © 2013 Elsevier Ltd. All rights reserved.
http://dx.doi.org/10.1016/j.carbpol.2013.05.010

morphology, transparency, viscosity, mechanical properties, and thermal expansion of the resulting nanofibers. While the electrospinning process is a "bottom-up" approach because it bundles molecules into nanofibers, the Star Burst process is considered to be a "top-down" approach. Utilizing the Star Burst system to create these nanofibers has several advantages over the electrospinning approach, including its low energy costs, high-volume production, organic solvent-free system, and excellent formability (Ifuku & Saimoto, 2012).

2. Experimental

2.1. Materials

Chitosan powder (cat. no. C0831, Mw: 420,000, degree of deacetylation: 78%) was purchased from Tokyo Chemical Industry and washed with water by filtration prior to use.

2.2. Preparation of chitosan nanofibers

Purified chitosan powder was dispersed in water at 1 wt.%. The dispersion was roughly crushed with a grinder (MKCA6-3; Masuko Sanyo Co., Ltd.) at 1500 rpm. The crushed dispersion was passed through the Star Burst system (Star Burst Mini, HJP-25001S, Sugino Machine Co., Ltd.) equipped with a ball-collision chamber. The slurry was ejected from a small nozzle with a diameter of 100 μm under high pressure of 245 MPa and collided with a ceramic ball with a diameter of 12.7 mm. The suspension was passed through 1, 5, 10, 30, and 50 mechanical treatments.

2.3. Preparation of chitosan nanofiber sheets

Nano-fibrillated chitosan nanofiber suspensions were dispersed in distilled water at a fiber content of 0.1 wt.%. The diluted suspensions were vacuum-filtered using a membrane filter. The obtained chitosan nanofiber sheets were dried by hot-pressing at 100 °C for 30 min. The dried sheets were cut into 5 cm × 5 cm squares with an approximate thickness of 29 μm and a weight of approximately 70 mg.

2.4. Characterization

Infrared spectra of the samples were recorded with an FT-IR spectrophotometer (Spectrum 65, Perkin-Elmer Japan Co., Ltd.) equipped with an ATR attachment. For field emission scanning electron microscopic (FE-SEM) observations, the prepared nanofiber suspension was diluted with ethanol and dried in an oven to obtain a chitosan nanofiber cast film. The film was coated with an approximately 2-nm layer of platinum using an ion sputter coater, and was observed by FE-SEM (JSM-6700F; JEOL, Ltd.) operating at 2.0 kV. Average diameters of the isolated nanofibers were evaluated by image analyses of at least 50 nanofibers. X-ray diffraction profiles of the nanofibers were obtained with Ni-filtered CuKα from an X-ray generator (Ultima IV, Rigaku) operating at 40 kV and 30 mA. The diffraction profile was detected using an X-ray goniometer scanning from 5° to 40°. The crystalline index (CI) was determined by following the equation: $CI = (I_{110} - I_{am}) \times 100/I_{110}$, where I_{110} is the maximum intensity ($2\theta = 20°$) of the 1 1 0 lattice diffraction and I_{am} is the intensity of the amorphous diffraction at 15.4° (Prashanth, Kittur, & Tharanathan, 2002). The light transmittances of chitosan nanofiber suspensions with 0.1 wt.% were measured using a UV–vis spectrophotometer (V550; JASCO, Tokyo, Japan). The viscosity of the chitosan nanofiber suspensions with 1.0 wt.% was measured using a Brookfield digital viscometer DV-E using spindle no. LV-4 (Brookfield Engineering Laboratories, Middleboro, MA). Determination of the Young's modulus and tensile strength of sheets was carried out using a universal testing instrument (AG-X, Shimadzu, Tokyo, Japan) for samples 50 mm in length and 10 mm in width. The nanofiber sheets of at least five specimens were tested. The coefficients of thermal expansion (CTE) of the sheets were measured with a thermometer analyzer (Q400, TA Instruments, Newcastle DE). Specimens were 30 mm in length and 3 mm in width, with a span of 20 mm. The measurements were carried out from 30 to 165 °C by elevating the temperature at a rate of 5 °C min^{-1} in a nitrogen atmosphere in tensile mode under a load of 0.05 N. The CTE values were determined in the second run after drying the samples completely in the first run.

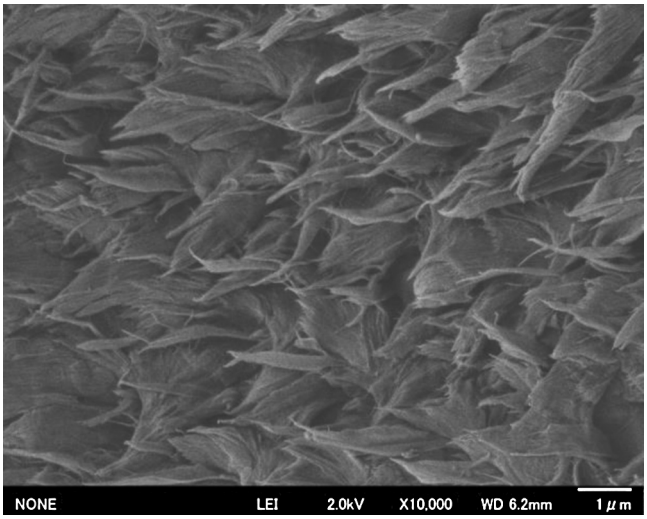

Fig. 1. FE-SEM micrographs of chitosan flakes.

3. Results and discussion

3.1. Observation of chitosan nanofibers

It is known that crab shell is made up of an aggregation of chitin nanofibers (Ifuku et al., 2009). Fig. 1 shows a surface image of the chitosan powder used in this study. Characteristic fibrous morphology was observed after deacetylation, suggesting that nanofibers may be obtained from chitosan powder after breaking down its structure. Fig. 2 shows the FE-SEM micrographs of a chitosan after Star Burst treatment with 0, 1, 5, 10, 30, and 50 passes in distilled water. In Fig. 2(a), we can see that the chitosan powder, having been roughly crushed by a grinder, has a fibrous structure. The thick aggregate of fibrous chitosan was broken down further into a mixture of micro- and nano-sized fibers after only one pass of the Star Burst treatment (Fig. 2(b)). After 5 passes, the fiber width decreased further due to fibrillation of the micron-sized fibers (Fig. 2(c)), although a small number of fibers approximately 100 nm in width remained. After 10 passes, most of the chitosan aggregate was well-fibrillated into fibers on the scale of tens-of-nanometers and had a very fine nanofiber network. Further mechanical treatments resulted in no significant changes in nanofiber formation, although the average fiber diameters decreased to some extent, from 40.8 nm (10 passes) to 36.6 nm (30 passes) and 34.8 nm (50 passes). In conclusion, the nanofiber morphology correlated strongly with the number of passes up until 10 passes. This result indicates that the chitin nanofiber aggregate structure was still maintained after deacetylation of chitin, which allows nano-fibrillation of chitosan powder. In contrast, we found that chitosan nanofibers could not be obtained from regenerated chitosan prepared by regeneration from chitosan solution in aqueous acetic acid.

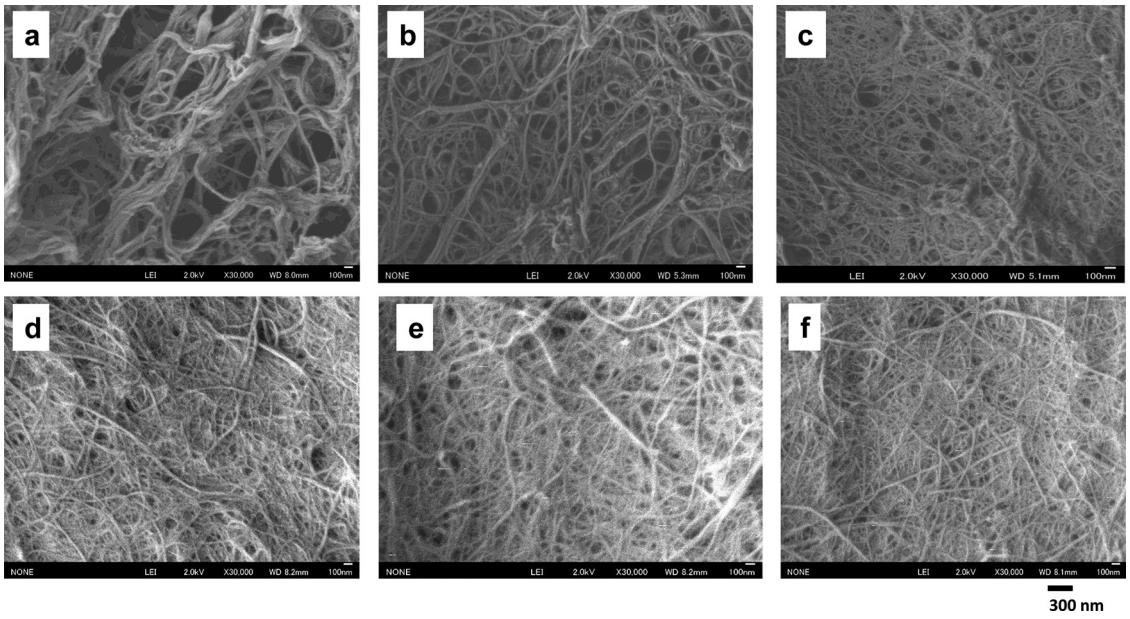

Fig. 2. FE-SEM micrographs of chitosan fibers after (a) 0, (b) 1, (c) 5, (d) 10, (e) 30, and (f) 50 passes through the Star Burst system.

3.2. Chemical and crystalline structures of chitosan nanofibers

The FT-IR spectra were used to evaluate the chemical structures of chitosan fibers processed after 0, 1, 5, 10, 30, and 50 passes by the Star Burst system. Chitosan nanofibers exhibited a number of absorbance peaks assigned to an OH stretching band at 3445 cm^{-1} overlapping an NH stretching band, and a CH stretching band at 2872 cm^{-1}. The amide I bands at 1652 and 1621 cm^{-1}, and the amide II band at 1554 cm^{-1} were derived from the *N*-acetylglucosamine unit of chitosan. All spectra of the obtained nanofibers were in excellent agreement with the spectrum of the original chitosan powder (data not shown). These results suggest that the Star Burst system retains the original chemical structure of chitosan, even after 50 passes.

Wide-angle X-ray diffraction was used to examine the crystalline structure of the fibrillated nanofibers by the Star Burst system after several passes. All chitosan samples showed major reflection at $2\theta = 9^\circ$ and 20°, which corresponds to 0 2 0 and 1 1 0 reflections, respectively (Prashanth et al., 2002). The peaks appeared at about the same reflection plane in each sample. Fig. 3 represents the relative degrees of crystallinity of chitosan nanofibers determined from the X-ray diffraction profiles. It was found that the relative degree of crystallinity decreased linearly from 48.1% (0 pass) to 39.5% (50 passes) after the Star Burst processes. These results indicate that Star Burst treatments damage the crystalline part of the chitosan fibers, likely due to the system employing a super high-pressure water jet of 245 MPa. The crystallinity of chitosan is considerably lower than that of chitin (Ifuku et al., 2012).

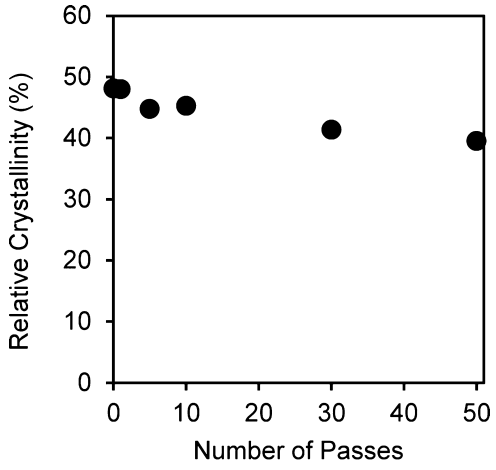

Fig. 3. Degree of relative crystallinity of chitosan nanofibers as a function of the number of passes.

3.3. Transparency and viscosity of chitosan nanofiber suspensions

The regular light transmittances of a fibrillated chitosan nanofiber slurry with a 0.1 wt.% concentration at a 600 nm wavelength are shown in Fig. 4 graphed against the number of passes. Since transparency is strongly associated with the chitosan fiber thickness, we can see the morphological change of chitosan nanofibers after Star Burst treatments from the data (Fan, Saito, & Isogai, 2008). That is, when solid fibers were dispersed at the nano level, the suspension became transparent. At 0 passes, the chitosan was not dispersed, but precipitated in water. At 1–10 passes,

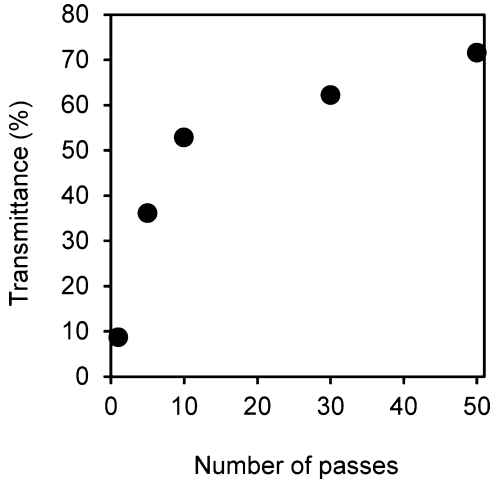

Fig. 4. Regular light transmittance of a chitosan nanofiber suspension at 600 nm as a function of the number of passes.

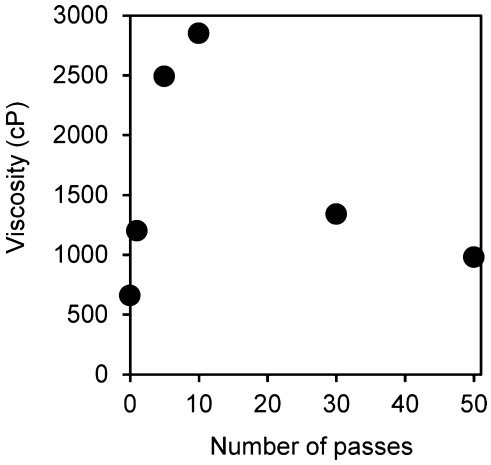

Fig. 5. Viscosity of chitosan nanofiber suspensions as a function of the number of passes.

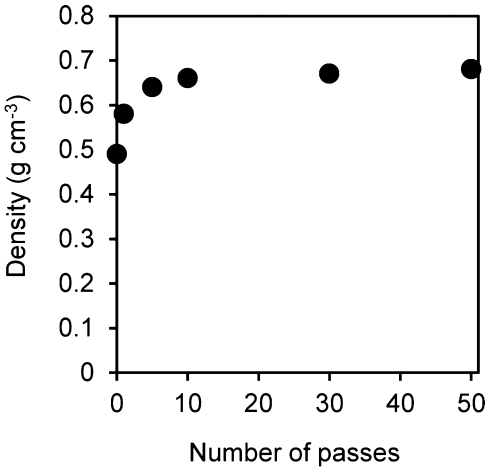

Fig. 6. Density of chitosan nanofiber sheets as a function of the number of passes.

the light transmittance of the chitosan slurry increased steeply from 8.6 to 52.8%, respectively. Above 10 passes, the increase in transmittance became more gradual; these results suggest that up until 10 passes the chitosan fibers were fibrillated regularly into thinner nanofibers. Above 10 passes, however, the chitosan was so fibrillated that it was difficult to achieve significant disintegration in response to further passes, resulting in a saturated transparency. These trends agree well with the FE-SEM observations. After the Star Burst treatment, chitosan nanofibers were dispersed homogeneously in water for at least 1 month, although conventional chitosan powder precipitated in water immediately. Chitosan nanofibers can therefore be easily mixed with other products and shaped into the desired forms.

Fig. 5 shows the viscosities of the chitosan nanofiber slurries with 1.0 wt.% concentration fibrillated by the Star Burst system as a function of the number of passes. The viscosity of zero-pass chitosan nanofibers is 657 cP. After Star Burst treatment, the viscosity increases steeply with increases in the number of passes, reaching 2850 cP at 10 passes. In contrast, above 10 passes, the viscosity decreases abruptly to 980 cP at 50 passes. The nanofiber morphology is closely linked to viscosity. That is, the thinner and longer the chitosan nanofibers, the more frequently they become entangled, thus increasing the viscosity. The viscosity data indicate that, up to around 10 passes, the nanofibers become thinner as the number of passes increases. After 10 passes, however, the nano-fibrillation decreases remarkably, as do the fiber lengths, thereby lowering the viscosity. These results are in good agreement with those obtained from the FE-SEM images.

3.4. Characterization of chitosan nanofiber sheets

Since the chitosan nanofibers were homogeneously dispersed in water, nanofiber sheets were easily prepared by vacuum filtration. Fig. 6 represents the density of the chitosan nanofiber sheets as a function of the number of passes. The density sharply increases from 0.49 to 0.66 g cm^{-3} at 0–10 passes, respectively. After 10 passes, the value seems saturated. The sheet density is associated with the chitosan nanofiber morphology. That is, the thinner the chitosan nanofibers, the more densely the nanofibers are packed in the sheet.

Fig. 7 displays the Young's moduli and tensile strengths of the chitosan nanofiber sheets graphed against the number of passes, respectively. Both Young's moduli and the fracture strengths of the chitosan nanofiber sheets increase with increases in the number of passes, reaching their peaks at 10 passes at 3535 MPa and 59.9 MPa, respectively. These values begin to decrease gradually above 10 passes, reaching 2828 MPa and 36.1 MPa, respectively, at 50 passes. In general, the mechanical properties of the nanofiber sheets were found to be related to the nanofiber width. When the chitin were fibrillated into a number of nanofibers, the chance of hydrogen-bonding interactions between nanofibers on the sheet increased. Therefore, the mechanical properties of the chitosan nanofiber sheet improved. Of course, the sheet density was also found to affect these mechanical properties (Fig. 6). Above 10 cycles, however, the length and crystallinity of the chitosan nanofibers decreased, as mentioned above, resulting in a direct deterioration of the mechanical properties of the sheets.

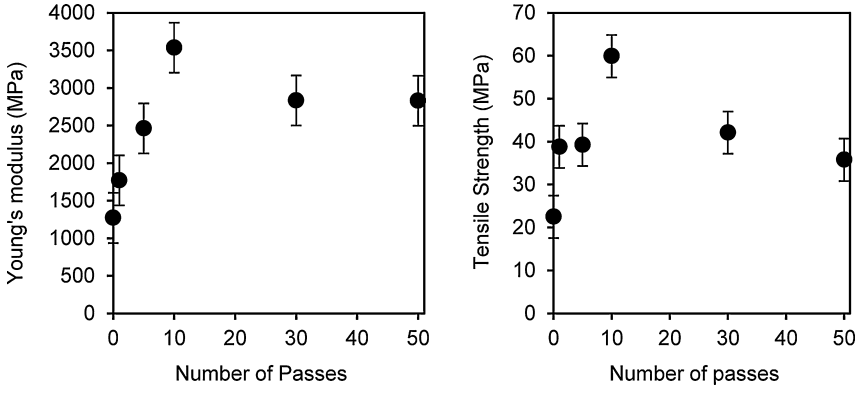

Fig. 7. Young's moduli and tensile strengths of chitosan nanofiber sheets as a function of the number of passes.

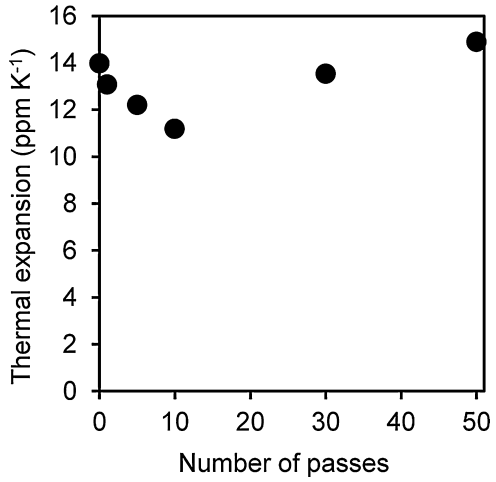

Fig. 8. Coefficient of thermal expansion of chitosan nanofiber sheets as a function of the number of passes.

Fig. 8 shows the coefficient of thermal expansion (CTE) values of the chitosan nanofiber sheets. The CTE decreased from 14.0 ppm K^{-1} at 0 passes to 11.2 ppm K^{-1} at 10 passes. In contrast, above 10 passes, the CTE increased abruptly, reaching 14.9 ppm K^{-1} at 50 passes. CTE is affected by the morphology and crystallinity of nanofibers. Up to 10 passes, the nanofibers became thinner with additional passes. The fine nanofiber network extending outward in a random manner resulted in a thermal expansion of the nanofibers in all directions, thus reducing the thermal expansion of the sheet. On the other hand, extensive Star Burst treatment reduced the crystallinity of the nanofibers, which directly increased the thermal expansion.

4. Conclusion

We studied the effects of the nano-fibrillation of chitosan by the Star Burst system, paying particular attention to the morphology, chemical structure, crystallinity, viscosity, mechanical properties, and thermal expansion of chitosan nanofibers. The chitosan powders turned into thinner nanofibers through the Star Burst system, as the nanofiber aggregate structure was still maintained after deacetylation treatment. Extensive cycles of treatment reduced the fiber length and crystallinity due to the high collision force caused by super high-pressure water. As a result, the mechanical and thermal expansion properties were improved by nanofibrillation up to 10 passes, while further treatment resulted in a degradation of these properties. We expect that this detailed characterization will play an important role in developing commercial applications for the nanofibers. The Star Burst system is advantageous from the perspective of its low energy costs, high-volume production, organic solvent-free system, and excellent formability. Naturally rare cationic-charged nanofibers can be obtained from chitosan flakes. The Star Burst system could therefore be a key tool for designing smart materials by means of ionic complex or self-organization approaches. Here, in addition to the chitin and cellulose nanofibers, the chitosan nanofibers have been now listed in bio-nanofibers.

Acknowledgement

This work was financially supported by KAKENHI (23750256) of JSPS.

References

Chen, P. Y., Lin, A. Y. M., McKittrick, J., & Meyers, M. A. (2008). Structure and mechanical properties of crab exoskeletons. *Acta Biomaterialia*, *4*, 587–596.

Duan, B., Dong, C., Yuan, X., & Yao, K. (2004). Electrospinning of chitosan solutions in acetic acid with poly(ethylene oxide). *Journal of Biomaterials Science Polymer Edition*, *15*, 797–811.

Fabritius, H., Sachs, C., Raabe, D., Nikolov, S., Friák, M., & Neugebauer, J. (2011). Chitin in the exoskeletons of arthropoda: From ancient design to novel materials science. In S. N. Gupta (Ed.), *Chitin* (34) (pp. 35–60). Netherlands: Springer.

Fan, Y., Saito, T., & Isogai, A. (2008). Preparation of chitin nanofibers from squid pen β-chitin by simple mechanical treatment under acid conditions. *Biomacromolecules*, *9*, 1919–1923.

Huang, Z. M., Zhang, Y. Z., Kotaki, M., & Ramakrishna, S. (2003). A review on polymer nanofibers by electrospinning and their applications in nanocomposites. *Composites Science and Technology*, *63*, 2223–2253.

Ifuku, S., Nogi, M., Abe, K., Yoshioka, M., Morimoto, M., Saimoto, H., et al. (2009). Preparation of chitin nanofibers with a uniform width as α-chitin from crab shells. *Biomacromolecules*, *10*, 1584–1588.

Ifuku, S., Nogi, M., Yoshioka, M., Morimoto, M., Yano, H., & Saimoto, H. (2011). Fibrillation of dried chitin into 10–20 nm nanofibers by a simple grinding method under acidic conditions. *Carbohydrate Polymers*, *84*, 134–139.

Ifuku, S., Yamada, K., Morimoto, M., & Saimoto, H. (2012). Nano-fibrillation of dry chitin powder by Star Burst system. *Journal of Nanomaterials*, *2012*, 1–7.

Ifuku, S., & Saimoto, H. (2012). Chitin nanofibers: Preparations, modifications, and applications. *Nanoscale*, *4*, 3308–3318.

Dutta, A. K., Yamada, K., Izawa, H., Morimoto, M., Saimoto, H., & Ifuku, S. (2013). Preparation of chitin nanofibers from dry chitin powder by Star Burst system: Dependence on number of passes. *Journal of Chitin and Chitosan Science*, *1*, 1–6.

Kose, R., & Kondo, T. (2011). Favorable 3D-network formation of chitin nanofibers dispersed in water prepared using aqueous counter collision. *Sen-I Gakkaishi*, *67*, 91–95.

Lee, K. Y., Jeong, L., Kang, Y. O., Lee, S. O., & Park, W. H. (2009). Electrospinning of polysachharides for regenerative medicine. *Advanced Drug Delivery Reviews*, *61*, 1020–1032.

Li, D., & Xia, Y. (2004). Electrospinning of nanofibers: Reinventing the wheel? *Advanced Materials*, *16*, 1151–1170.

Lin, T., Fang, J., Wang, H., Cheng, T., & Wang, X. (2006). Using chitosan as a thickener for electrospinning dilute PVA solutions to improve fiber uniformity. *Nanotechnology*, *17*, 3718–3723.

Min, B., Lee, S. W., Lim, J. N., You, Y., Lee, T. S., Kang, P. H., et al. (2004). Chitin and chitosan nanofibers: Electrospinning of chitin and deacetylation of chitin nanofibers. *Polymer*, *45*, 7137–7142.

Muzzarelli, R. A. A. (2011). Chitin nanostructures in living organisms. In S. N. Gupta (Ed.), *Chitin formation and diagenesis* (34) (pp. 1–34). Dordrecht: Springer.

Muzzarelli, R. A. A., Boudrant, J., Meyer, D., Manno, N., DeMarchis, M., & Paoletti, M. G. (2012). Current views on fungal chitin/chitosan, human chitinases, food preservation, glucans, pectins and inulin: A tribute to Henri Braconnot, precursor of the carbohydrate polymers science on the chitin bicentennial. *Carbohydrate Polymers*, *87*, 995–1012.

Muzzarelli, R. A. A. (2012). Nanochitins and nanochitosans, paving the way to eco-friendly and energy-saving exploitation of marine resources. In K. Matyjaszewski, & M. Möller (Eds.), *Polymer science: A comprehensive reference* (10) (pp. 153–164). Amsterdam: Elsevier B.V.

Nikolov, S., Fabritius, H., Petrov, M., Friák, M., Lymperakis, L., Sachs, C., et al. (2011). Robustness and optimal use of design principles of arthropod exoskeletons studied by ab initio-based multiscale simulations. *Journal of the Mechanical Behavior of Biomedical Materials*, *4*, 129–145.

Peter, M. G. (1995). Applications and environmental aspects of chitin and chitosan. *Journal of Macromolecular Science, Part A: Pure and Applied Chemistry*, *32*, 629–640.

Prashanth, K. V. P., Kittur, F. S., & Tharanathan, R. N. (2002). Solid state structure of chitosan prepared under different *N*-deacetylating conditions. *Carbohydrate Polymers*, *50*, 27–33.

Raabe, D., Sachs, C., & Romano, P. (2005). The crustacean exoskeleton as an example of a structurally and mechanically graded biological nanocomposite material. *Acta Materialia*, *53*, 4281–4292.

Raabe, D., Romano, P., Sachs, C., Fabritius, H., Al-Sawalmih, A., Yi, S. B., et al. (2006). Effect of microstructure on anisotropy of mineralized cuticle from the lobster Homarus americanus. *Materials Science and Engineering A*, *421*, 143–153.

Rao, S. B., & Sharma, C. P. (1997). Use of chitosan as a biomaterial: Studies on its safety and hemostatic potential. *Journal of Biomedical Materials Research*, *34*, 21–28.

Sill, T. J., & Recum, H. A. (2008). Electrospinning: Applications in drug delivery and tissue engineering. *Biomaterials*, *29*, 1989–2006.

Xia, Y., Yang, P., Sun, Y., Wu, Y., Mayers, B., Gates, B., et al. (2003). One-dimensional nanostructures: Synthesis, characterization, and applications. *Advanced Materials*, *15*, 353–389.